Harmonics Free Voltage Stability Enhancement By Multi-Level Inverter Unified Power Flow Controller

دعم إستقرار الجهد بدون توافقيات بإستخدام متحكم متوحد لتدفق القدرة الكهربية ذو عاكس متردد متعدد المستويات

Mohammed El Gamal
SUMED Co., Alex., Egypt
m_sumed@yahoo.com

Ahmed Lotfy
AASTMT, Egypt
alotfy@aast.edu

G. E. M. Ali
Tanta University, Egypt

ملخص - تمت محاكاة متحكم متوحد لتدفق القدرة الكهربية ذو عاكس متردد متعدد المستويات وإستخدامه فى الحفاظ على استقرار مستوى الجهد الخاص بخط نقل للقدرة الكهربية و حمايته من الارتفاع أو الهبوط عن الحد المقنن للخط. وقد تم تصميم هذا المتحكم كوحدة واحدة مستقلة و تم اختباره ببرنامج الباسكاد حيث تمت محاكاة العديد من حالات التشغيل المعتادة والعابرة لإختبار قوة و سرعة استجابة هذا المتحكم فى الحفاظ على مستوى الجهد تحت ظروف التشغيل المختلفة.

Abstract -A multi-level inverter based unified power flow controller system is modeled and applied in a transmission line to maintain voltage stability and protect / compensate against over-voltages, under-voltages, sags and swells. The controller is designed as a stand-alone module and tested in PSCAD-EMTDC environment where different normal and abnormal operating conditions were simulated to validate the robustness of the controller and its capability to rapidly maintain voltage stability under different load conditions.

Key words - Multilevel inverter, UPFC, voltage stability.

1. INTRODUCTION

Unified Power Flow Controllers (UPFC) are the most versatile and complex power electronic equipment applied for the control and power flow optimization in electrical power transmission systems. It offers major potential advantages for the static and dynamic operation of transmission lines. Nevertheless, it brings with it major design challenges, both in the power electronics and from the prospective of application to power systems. The transmission line containing the UPFC appears to the rest of the power system as a high impedance power source or sink; an extremely powerful mode of operation that has not previously been achievable. Due to the continuously increasing demand for electrical energy, and the restricted locations for generation, transmission lines are becoming overloaded and experiencing reduced stability, increased voltage variation, and "loop-flow" of power. The construction of new transmission lines is becoming increasingly difficult forcing constant search for economic ways to transfer bulk power along a desired path. The utilization of existing transmission systems should thus be limited by thermal and not stability limits. The UPFC combines the functions of several FACTS devices and is capable of implementing voltage regulation, series compensation, and phase angle regulation at the same time, thus realizing the separate control of the active power and reactive power transmitted simultaneously over the line. The UPFC thus provides effective means for controlling the power flow and improving the transient stability in a power network. Description of basic control, sequencing and protection philosophies that govern the operation of the UPFC is explained in [1]. The theory and modeling technique of unified power flow controller using an electromagnetic transient program (EMTP) simulation package is described in [2]. Modeling the UPFC in the harmonic domain and for power flow, voltage, angle and impedance controls is presented in [3 & 4]. A platform system, global control and comprehensive UPFC analysis is described in [5, 6 & 7]. Laboratory experimental models of UPFC systems were proposed in [8, 9 & 10]. The use of UPFC in power flow control and power system transient stability improvement is depicted in [11, 12, 13 & 14].

So far most of the literature reviewed implemented classical techniques with linearized mathematical models of UPFC and transmission lines, which are considered to some extent inaccurate for control simulation of the UPFC. Some trials have been made to use artificial intelligent techniques like fuzzy logic control to simulate UPFC control. But these trials have been focused on simulation programs that support fuzzy control [15, 16 & 17]. In [18] ATP-EMTP program is used to simulate an FL controller capable of enhancing the dynamic performance of the UPFC. In [19], numerical simulation of New England power system is used to demonstrate the role of FL control of the UPFC in power system stability enhancement.

In this paper, transmission line voltage stability is achieved by a UPFC to accurately interact with system nonlinearities. The proposed technique is built and tested under PSCAD-EMTDC environment. The UPFC shunt and series converters are each constructed as "seven - level" diode clamped converters.

Accepted July 8, 2011.

2. TRANSMISSION LINE AND UPFC MODELS

UPFC comprises a shunt connected static synchronous compensator (STATCOM) and a static synchronous series compensator (SSSC). The STATCOM and SSSC parts of the UPFC are constructed from two back to back voltage and phase shift controlled seven - level diode clamped multilevel converters with a common DC link constructed from six capacitors. The UPFC is inserted in a transmission line system as shown in Fig. 1.

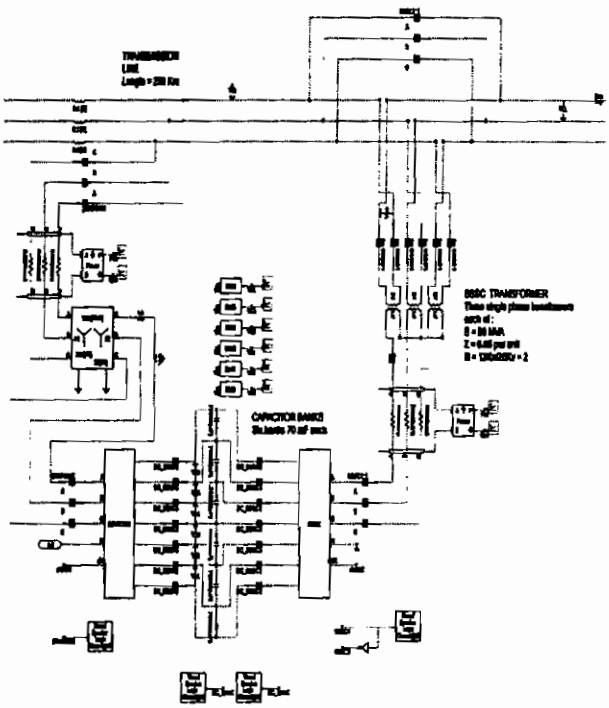

Figure 1 Transmission line and UPFC Model

The topology of one leg of the modeled UPFC inverters comprising 10 clamping diodes and 12 switching devices with anti parallel diodes in each arm is shown in Fig. 2. During the voltage regulation mode of SSSC part, the STATCOM part of the UPFC is controlled to maintain the UPFC capacitors charged to the rated level irrespective of the active power delivered or received from the SSSC part. The shunt transformer steps down the 220 kV bus voltage to 22 kV at the terminals of the inverter. Various operating conditions of the transmission line may cause under-voltage, over-voltage, sag or swell; the SSSC part is controlled to maintain the UPFC bus voltage level within allowable limits by injecting voltage in or out of phase with respect to the sending end voltage. The UPFC bus line voltage is first sensed by voltage transformers to trigger one of two cases; when the line voltage is just exceeding 220 kV, and when it is just less than 220 kV. When the first case is encountered, the SSSC voltage will be inserted in phase opposition to the UPFC bus line voltage with the appropriate modulation index. On the contrary, in the second case the voltage will be just in phase with the UPFC line voltage with certain modulation index. The SSSC controller will determine the modulation index for each case according to the severity of under/over voltage.

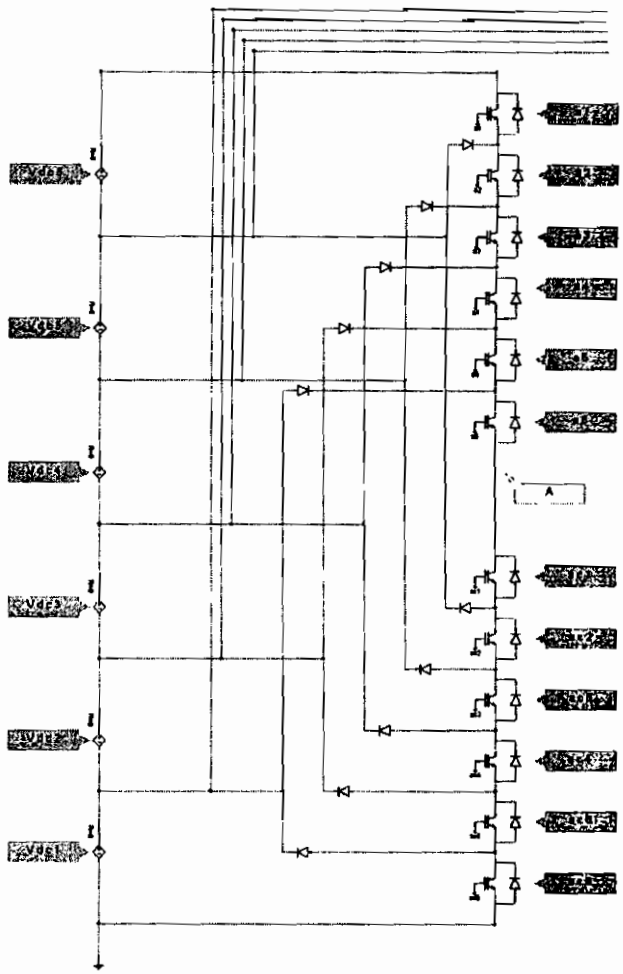

Figure 2 One arm of seven-level diode clamped inverter

3. UPFC capability validtion

To validate the capability of the proposed multi-level inverter based unified power flow controller to maintain the transmission line system voltage stability, various normal and abnormal operating conditions are simulated. Accordingly, the P-V and Q-V curves of the UPFC bus voltage are plotted in cases where the UPFC action is inhibited or activated. The behavior during sag conditions is investigated without and with controller action by connecting a load of 100 + j 300

MVA to the line at t = 0.3 S. To further investigate the transmission line behavior during swell conditions, the system is operated with bus voltage stabilized to the allowed limits to supply three loads; the first and second loads are 50 + j100 MVA each, and the third load is 50 + j150MVA. At t = 0.3 S, the third load is disconnected from the line causing line over voltage and at t = 0.4 S the second load is further disconnected causing line voltage swell.

4. Results and discussion

Fig. 3 shows the Q-V curves with and without UPFC. It is evident that heavy loading of the line (250 MW / 400 MVAR) without using UPFC, decreases the transmission line voltage to 162 kV.. Nevertheless, inserting UPFC in line with the same loading hinders the voltage from going below 211.5 kV.

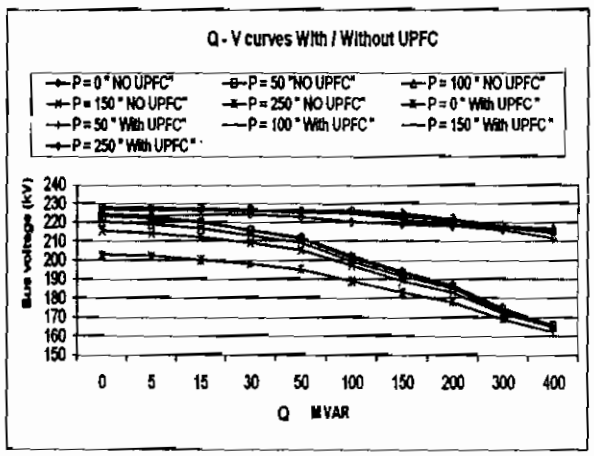

Figure 3 Q-V curves with & without UPFC

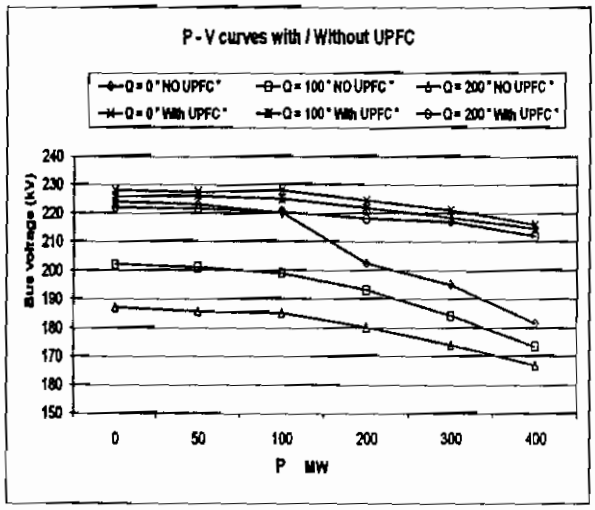

Figure 4 P-V curves with & without UPFC

Fig. 4 shows the P-V curves without and with UPFC respectively. It is clear that at heavy loading of the line (400 MW / 200 MVAR) without UPFC, the transmission line voltage reaches 167 kV. Nevertheless, inserting UPFC in line with the same loading hinders the voltage from going below 212 kV.

As shown in Fig. 5, during the sag condition without the UPFC, the bus voltage drops to 173 kV. When UPFC is activated, the lowest value of line voltage reached after three quarters of a cycle of load insertion is 210 kV, after two and a half cycles it is fully regulated.

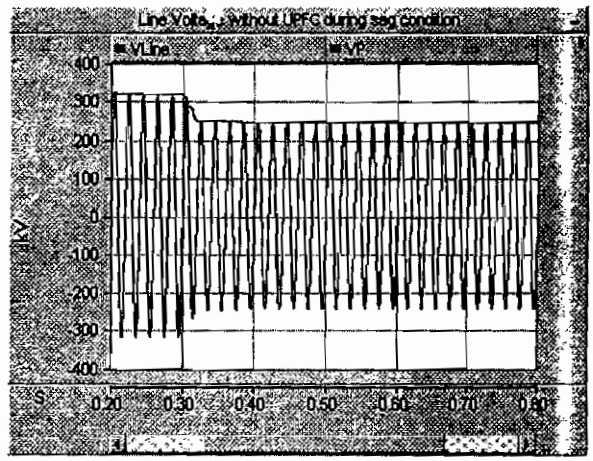

(a) Sag condition without UPFC

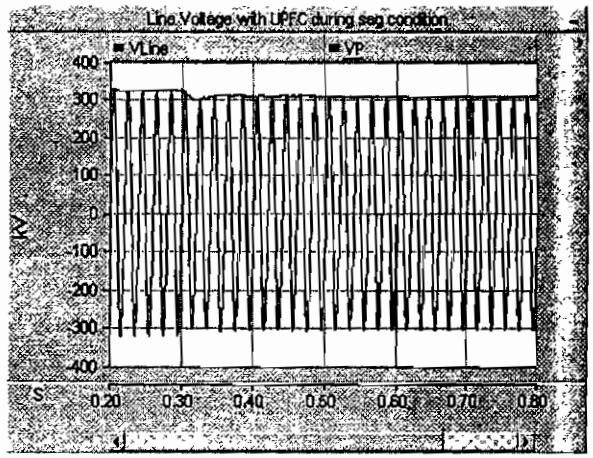

(b) Sag condition with UPFC

Figure 5 Sag condition without & with UPFC

As shown in Fig. 6, the associated UPFC bus voltage total harmonic distortion (THD*v*) is 1.47 %, and the associated transmission line total current harmonic distortion (THD*i*) is 0.54 %, both of which are within allowable limits.

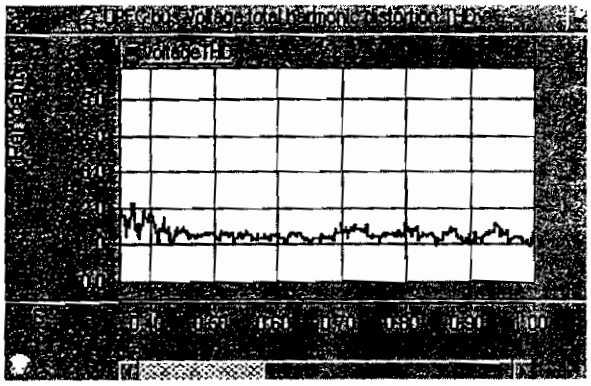

(a) THDv during sag override

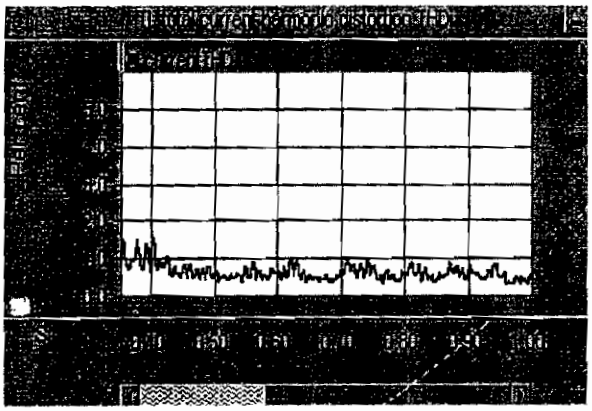

(b) THD*i* during sag override

Figure 6 Total harmonic distortion during sag override

The controller performance in terms of the modulation index of the SSSC part and capacitors' voltages are shown in Fig. 7 and Fig. 8 respectively; the figures show the controller fast response of MI and proper balancing of the capacitor banks' DC voltages. During the swell condition, Fig. 9 shows the transmission line bus voltage with and without UPFC.

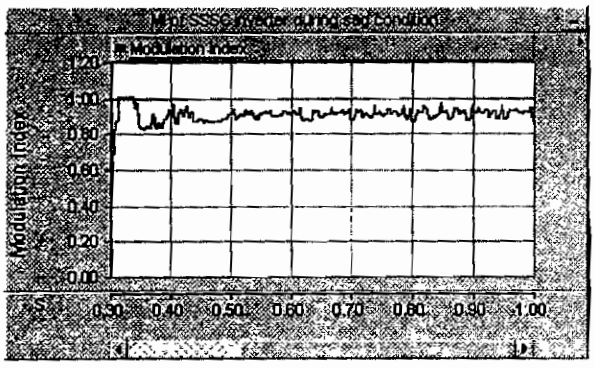

Figure7 Modulation index of SSSC during sag override

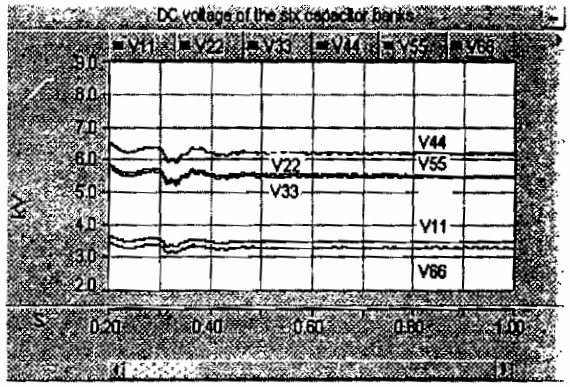

Figure 8 DC capacitor voltages during sag override

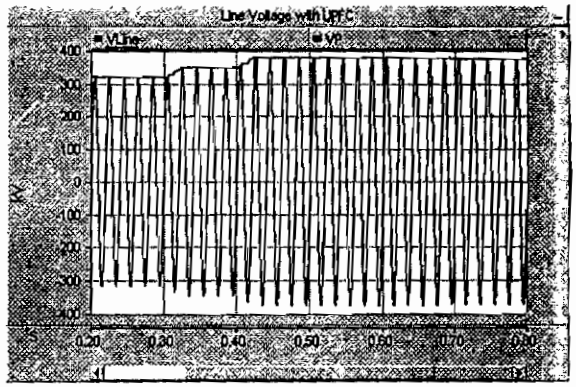

(a) Swell without UPFC

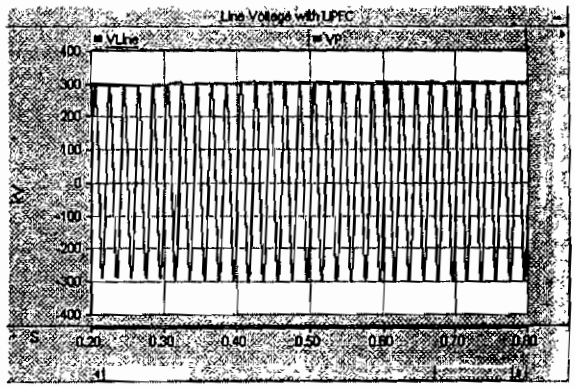

(b). Swell with UPFC

Figure 9 Swell without and with UPFC

Fig. 10 shows that total harmonic distortion associated with swell override are still within allowable limits. The controller performance in terms of both of the modulation index of the SSSC part and the resulting capacitor voltages are shown in Fig. 11 and Fig. 12.

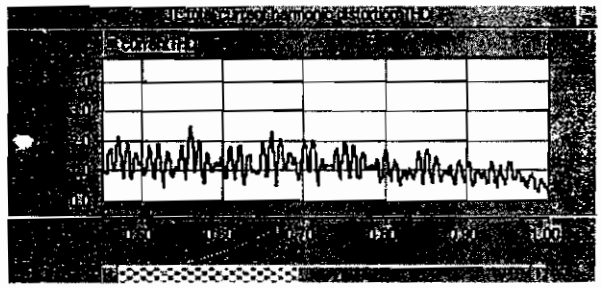

(a) THDi during swell override

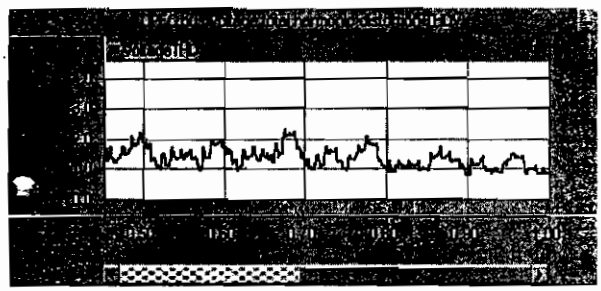

(b) THDv during swell override.

Figure 10 Total harmonic distortion during swell override

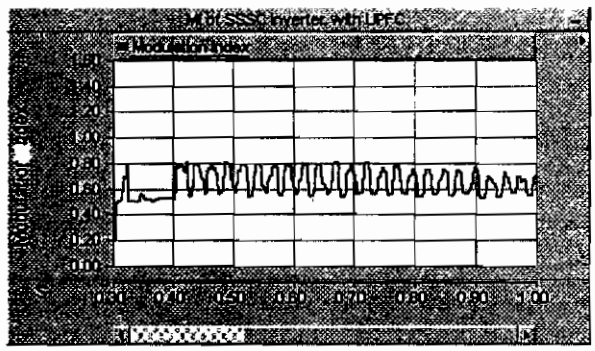

Figure 11 Modulation index of SSSC during swell override.

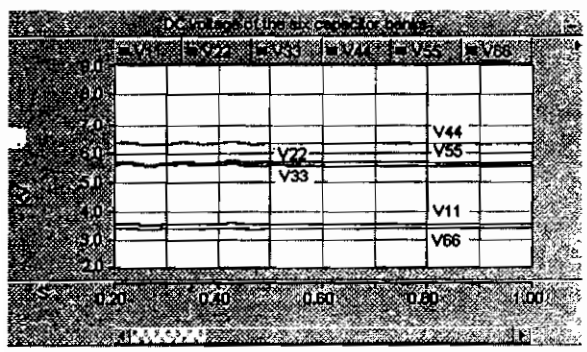

Figure 12 DC capacitor voltages during swell override.

5. Conclusion

The control of transmission line voltage stability is achieved by a UPFC built and tested under PSCAD-EMTDC environment. The controller utilizes multi-level inverter topology. The controller shows superior performance while maintaining power system quality indices during voltage disturbances in terms of total voltage and current harmonic distortions respectively due to the adoption of 'almost harmonic free' seven level diode clamped converters in both of the STATCOM and SSSC parts .

References

[1] Schauder, Hamai, Edris et al., "Operation of the unified power flow controller (UPFC) under practical constraint", IEEE transactions on power delivery, vol. 13, no. 2, April 1998.

[2] Sen and Stacey, "UPFC-unified power flow controller: theory, modeling and application", IEEE transactions on power delivery, vol.13, no.4, October 1998.

[3] Collins, Watson and Wood, "UPFC modeling in the harmonic domain", IEEE transactions on power delivery, vol. 21, no.2, April 2006.

[4] Dai and Liu, "Study on modeling of the unified power flow controller", proceedings of the IEEE international conference on automation and logistics, August 18-21, 2007, Jinan, China

[5] Jiang et al., "A platform for validation of FACTS models", IEEE transactions on power delivery, vol. 21, no. 1, January 2006.

[6] Mahdad, Bouktir and Srairi," The impact of unified power flow controller in power flow regulation", IEEE MELECON 2006, May 16-19, 2006 Benalamadena (Malaga),Spain.

[7] Fujita, Watanabe and Akagi, "Control and analysis of a unified power flow controller", IEEE transactions on power electronics, vol. 14, no. 6, November 1999.

[8] Chen et al., "Unified power flow controller (UPFC) based on chopper stabilized diode clamped multilevel converters", IEEE transactions on power electronics, vol.15, no.2, March 2000.

[9] Mwinyiwiwa, Lu and OOi, "Multiterminal unified power flow controller", IEEE transactions on power electronics, vol.15, no.6, November 2000.

[10] Fujita, Akagi and Watanabe, "Dynamic control and performance of a unified power flow controller for stabilizing an AC transmission system", IEEE transactions on power electronics, vol. 21, no.4, July 2006.

[11] Kannan, Jayaram and Salama, "Real and reactive power coordination for a unified power flow controller", IEEE transactions on power systems, vol.19, no.3, August 2004.

[12] Gholipour and Saadate, "Improving of transient stability of power system using UPFC", IEEE transactions on power delivery, vol.20, no. 2, April 2005.

[13] Azbe, Gabrijel, Povh and Mihalic, "The energy function of a general multimachine system with a unified power flow controller", IEEE transactions on power systems, vol. 20, no. 3, August 2005.

[14] Liu et al., "Power flow control performance analysis of a unified power flow controller in a novel control scheme", IEEE transactions on power delivery, vol. 22, no. 3,July2007.

[15] Mekri, Machmoum, Ahmed and Mazari, "A fuzzy hysteresis voltage and current control of an unified power quality conditioner", proc. industrial electronics society 34th annual conference, 2008, IECON08, pp 2648 - 2689.

[16] Farrag et al., "Design of fuzzy based rules control system for the unified power flow controller", proc. industrial electronics society 28th annual conference, 2002, IECON02, pp 2102 - 2107.

[17] Dejamkhooy et al., "Fuzzy logic based UPFC controller for damping low frequency oscillations of power systems", 2nd international conference on power and energy (PECon 08), December 1-3, 2008, Malaysia.

[18] Menniti, Pinnarelli and Sorrentino, "A novel fuzzy logic controller for UPFC", proc. int. conf. on power system technology, 2000, POWERCON2000, Vol. 2, pp 691 696.

[19] Prakash and Nair, "A robust control strategy of UPFC to improve transient stability using fuzzy bang bang control", proc. int. conf on computational intelligence and multimedia appliacations,vol1,2007, pp 352 - 356.

Mansoura Engineering Journal, (MEJ), Vol. 36, No. 3, September 2011. E. 14

Optimal Placement of PMU Using Improved Tabu Search for Complete Observability of Power System and Out of Step Prediction

تحديد المواقع المثلى لوحدات القياس الاتجاهى باستخدام البحث الممنوع المحسن لتحقيق الرؤية الكاملة لمنظومة القوى و توقع عدم اتزانها

Amany M.El-Zonkoly[1], Samah El-Safty[2] and Rana Maher
Department of Electrical & Control Engineering – Faculty of Engineering & Technology
Arab Academy for Science & Technology and Maritime Transport
Miami – Alexandria – Egypt – P.O. 1029
[1] amanyelz@yahoo.com , [2] drsamahsafty@yahoo.com

ملخص

تقدم الورقة البحثية طريقة لتحديد الموقع الأمثل لوحدات القياس الاتجاهى لتحقيق الرؤية الكاملة لمنظومة القوى. و تعتمد الطريقة المقترحة على الرؤية العددية و الذكاء الاصطناعى. و قد تم استخدام خوارزم ذكاء اصطناعى من نوع البحث الممنوع المحسن لتحديد الموقع الأمثل لوحدات القياس الاتجاهى للحفاظ على الرؤية الكاملة للمنظومة. كما تصف الورقة البحثية خوارزم لتوقع عدم اتزان المولدات مبنى على رؤية فارق جهد الوجه بين المحطات. و قد تم اختبار الخوارزمين على منظومتى **IEEE** ذات ستة قضبان و اربعة عشر قضيب و كذلك على شبكة ٥٠٠ ك ف المصرية. كما تم محاكاة نظم الاختبار و الخوارزمات المستخدمة باستخدام برامج **PSCAD** و **MATLAB**.

Abstract

This paper proposes an optimization method for optimal placement of phasor measurement units (PMUs) for complete observability of power system. The proposed method is based on numerical observability and artificial intelligence. The artificial intelligence algorithm used is the Improved Tabu Search (ITS) algorithm. The ITS is used to find the optimal placement for the PMU to keep the system complete observable. Also, the paper describes a predictive Out-Of-Step (OOS) algorithm based on the observation of the voltage phase difference between substations. The proposed optimal placement of PMUs and the OOS algorithms are tested using the IEEE 6 bus, IEEE 14 bus systems and the Egyptian 500 kV network. The test systems are simulated using the PSCAD software program. The placement algorithm and the OOS prediction algorithm are carried out using MATLAB script programs.

Keywords

Optimal placement of Phasor measurement units, Observability, Improved Tabu Search (ITS), Predictive Out-of-step Protection

1. Introduction

The phasor measurement units (PMUs) are measuring devices synchronized via signals from global positioning system (GPS) satellite transmission [1]. They are employed to measure the positive sequence of voltage and current phasors. By synchronized sampling of microprocessor-based systems, phasor calculations can be placed on a common reference. The magnitudes and angles of these phasors comprise the state of the power system and they are used in complete observability and transient stability analysis. The observability of a system can be assessed by considering the topology of the network and the types and locations of the measurements. Transient instability becomes more and more complicated as the power systems grow in more scale and complexity. OOS studies become more essential to prevent large scale black-out in power systems.

In recent years, there has been a significant research activity on the problem of finding the minimum number of PMUs and their optimal locations. In [2], a bisecting search method was implemented to find the minimum number of PMUs to make the system observable. In [3], the authors used a simulated annealing technique to find the optimal PMU locations. In [4], a genetic algorithm was used to find the optimal PMU locations. The

Accepted August 23, 2011.

minimum number of PMUs needed to make the system observable was found by using a bus-ranking methodology. In [5] and [6] the authors used integer programming to determine the minimum number of PMUs. The authors in [7] used the condition number of the normalized measurement matrix as a criterion for selecting candidate solutions, along with binary integer programming to select the PMU locations.

Various methods for the OOS detection have been developed and were in use in protection systems, such as tracking trajectory of the impedance vector measured at the generator terminals [8], rate of change of apparent resistance augmentation [9] or Liapunov theory [10].

The present paper first proposes an optimal search approach based on an improved tabu search (ITS) to determine the optimal locations of PMUs for complete system observability. Then the paper introduces a predictive OOS algorithm based on measuring the phase difference between several generators from voltage data collected at substation buses.

2. System Observability Analysis

The observability of a system can be assessed by considering the topology of the network and the types and locations of the measurements. The meter placement algorithm presented in this paper is based on the observability analysis method introduced earlier in [11] & [12]. This method will be briefly reviewed first.

2.1 Linear Size and Page Layout

Consider an N-bus system provided with m-measurements of voltage and current phasors contained in vector z. The vector z is linearly related to the N-dimensional state vector x containing N-nodal voltage phasors, resulting in n=2N - 1 state variables [11]. This yields the linear model

$$z = H x + e \qquad (1)$$

Where H is the (m * N) design matrix and e is an (m * 1) additive measurement error vector.

By splitting the vector z into the (m_V * 1) voltage and (m_I * 1) current subvectors, z_V and z_I,respectively. Also by splitting the vector x into the (N_M * 1) measured and (N_C * 1) nonmeasured sub-vectors, V_M and V_C, respectively, relationship (1) becomes

$$\begin{bmatrix} Z_V \\ Z_I \end{bmatrix} = \begin{bmatrix} 1 & 0 \\ Y_{IM} & Y_{IC} \end{bmatrix} \begin{bmatrix} V_M \\ V_C \end{bmatrix} + \begin{bmatrix} e_V \\ e_I \end{bmatrix} \qquad (2)$$

Where 1 is the identity matrix and Y_{IM} and Y_{IC} are sub-matrices whose entries are series and shunt admittances of the network branches.
When the shunt elements are neglected, then the design matrix H reduces to

$$H = \begin{bmatrix} 1 & 0 \\ M_{IB} Y_{BB} A_{MB}^T & M_{IB} Y_{BB} A_{CB}^T \end{bmatrix} \qquad (3)$$

where M_{IB} is the (m_I x b) measurement-to-branch incidence matrix associated with the current phasor measurements. Y_{BB} is the (b x b) diagonal matrix of the branch admittances. A_{MB} and A_{CB} are the (N_M x b) measured and (N_C x b) calculated node-to-branch incidence sub-matrices, respectively.

2.2 The Observability Check

The decoupled gain matrix for the real power measurements can be formed as [12]:

$$G = H^T H \qquad (4)$$

Note that, since the slack bus is also included in the formulation, the rank of H (and G) will be at most (N-1), even for a fully observable system. This leads to the triangular factorization of a singular and symmetric gain matrix.
The symmetric matrix G can be decomposed into its factors LDL^T where the diagonal factor D, may have one or more zeros on its diagonal. If it have more than one zero on its diagonal then the system is unobservable.

3. Tabu Search Algorithm

Tabu search (TS) algorithm is a powerful optimization procedure that has been successfully applied to a number of combinatorial optimization problems. It is an optimization method developed by F.Glover [13]-[14] specifically for combinational optimization problem. It guides the search for the optimal solution making the use of memory systems which exploit its past history and leads to the best solution. Fundamental concept of simple TS involves individual, population and generation. If v_k is the trial vector up to iteration k, Δv_k is a move, then $v_{k+1}=v_k+\Delta v_k$ is the trial vector at iteration k+1. The set of all possible moves out of a current solution is called the set of candidate moves. One could operate with a subset of it.

3.1 Tabu Restrictions

There are certain conditions imposed on moves, which make some of them forbidden. These forbidden moves are known as tabu. A tabu list will be formed to record these

moves. A new trial vector satisfies tabu restriction is classified as tabu. The dimension of the tabu list is called the *tabu list* size. Let v_{tabu} be any vector in the tabu list and d_{tabu} the tabu distance, for extending simple TS to the real-valued optimization problem, a tabu restriction in improved TS can be expressed as

$$|(v_k + \Delta v_k) - v_{tabu}| < d_{tabu} \quad (5)$$

3.2 Aspiration Criteria

Aspiration criteria can override tabu restrictions. That is, if a certain move is forbidden, the aspiration criteria, when satisfied, can reactivate this move. Let v^*_k be the best current solution, aspiration criteria can be expressed as (5) with

$$cost(v_k + \Delta v_k) < cost(v^*_k) \quad (6)$$

The ITS is a mixture of the simple TS and simple genetic algorithm (GA). The ITS is explained in details in [15].

4. Optimal PMU Placement Algorithm

The proposed algorithm will be applied to find the optimal measurement scheme such that the network will be fully observable. That is why the observability check will be carried out along with the tabu and aspiration checks for every individual of the population. The optimal scheme will represent the essential measurement set. The fitness value of an individual will be the cost of the PMUs placed.

The same procedure is repeated to find the locations of the extra PMUs needed to be placed in case of loss of a single PMU or the loss of a single branch of the branches of the system.

Such an application will lead to the required set of PMUs needed to keep the system fully observable under normal conditions and during the two contingencies of loosing any PMU or any branch.

A MATLAB program is developed to fulfill the logical steps of the ITS algorithm, starting from the initialization of the first populations, and ending with determining the optimal placement of PMUs all over the power network.

The algorithm procedures of ITS program can be summarized in the following steps;

1. Initiate a number of populations that is constrained to be completely observable.
2. Calculate the cost (fitness function) of each individual and sort them in an ascending order.

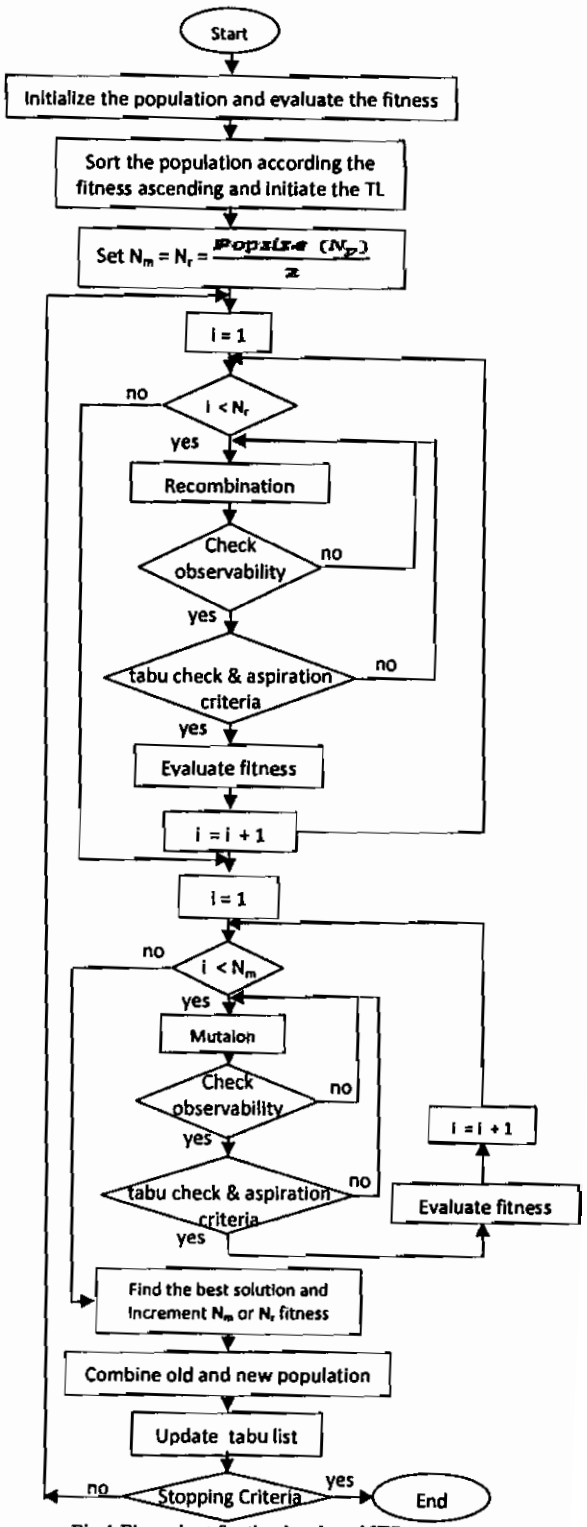

Fig.1 Flow chart for the developed ITS program

3. Pick up the first tabu list, with its tabu size set to maximum (τ_{max}), out of the sorted initial population.
4. Evaluate the constrained neighbors (new set of populations) through mutation and recombination.
5. Calculate the cost of each individual.
6. Check the tabu restriction and aspiration criteria.
7. Calculate the fitness and arrange all individuals in ascending order then pick up the new population.
8. Update all the adaptive parameters, e.g. N_m, N_r, τ, β and α.
9. Check the stopping criterion.

A flowchart for the developed ITS program is shown in Fig.1.

5. Optimal Placement Test Results

5.1 IEEE 6-Bus System

In case of the IEEE 6-Bus, the optimization algorithm yield to the result that the system needs PMUs located at bus 1 and bus 5 for complete observability under normal operation. Also, the ITS yield to the need of an extra PMU to be placed at bus 4 to guarantee the system observability in case of loss of any PMU or in case of the loss of any branch of the system.

5.2 IEEE 14-Bus System

In case of the IEEE 14-Bus, the optimization algorithm yield to the result that the system needs PMUs located at buses 2,6 and 9 for complete observability under normal operation.

Results of ITS in case of loss of a single PMU and in case of loss of a single branch are represented in Table 1 and Table 2, respectively. Table 2 shows only the branches that will cause the system to be unobservable when they are out of service. From Tables 1 and 2, it can be concluded that the extra PMUs that will keep the system observable in case of loss of any main PMU or loss of a branch are to be placed at buses 1, 7 and 13.

Table 1
The ITS results in case of loss of a single PMU

Out PMU at bus	Locations of extra PMUs
2	1, 7
6	7, 13
9	7, 13

Table 2
ITS results in case of loss of a single branch

Branch Out	Locations of extra PMUs
1-2	1
2-3	1
6-11	1, 7
6-12	13
6-13	7,13
7-9	13
9-10	1, 7
9-14	13

5.3 Egyptian 500 kV Network

In case of the Egyptian 500 kV network, the optimization algorithm yield to the result that the system needs PMUs located at buses 3, 7, 8 and 12 for complete observability under normal operation.

Results of ITS in case of loss of a single PMU and in case of loss of a single branch are represented in Table 3 and Table 4, respectively. From Tables 3 and 4, it can be concluded that the extra PMUs that will keep the system observable in case of loss of any main PMU or loss of a branch are to be placed at buses 1, 6, 10 and 11.

Table 3
The ITS results in case of loss of a single PMU

Out PMU at bus	Locations of extra PMUs
3	1, 11
7	6, 11
8	6, 10
12	1, 11

Table 4
ITS results in case of loss of a single branch

Branch Out	Locations of extra PMUs
1-2	6, 10
2-3	1, 6, 10
3-4	6
4-5	6
4-8	11
5-6	6
5-8	1
6-7	6
7-9	1, 6
8-10	1, 6
9-10	1, 6
9-11	6
11-12	6
12-13	6

6. Out-Of-Step Prediction Algorithm

The test systems are simulated using the PSCAD software program. Phase difference between several generators is detected from voltage data recorded at generators buses, and then phase difference is predicted in advance. If the predicted phase difference exceeds the instability threshold value, the system is considered to be unstable.

The OOS prediction algorithm is carried out using M-files MATLAB programs.

6.1 Calculations of Predicted Value for Phase Difference

In [16], authors used the phase difference values for the present time and previous time to predict the future phase difference value. This method will be described using Fig.2.

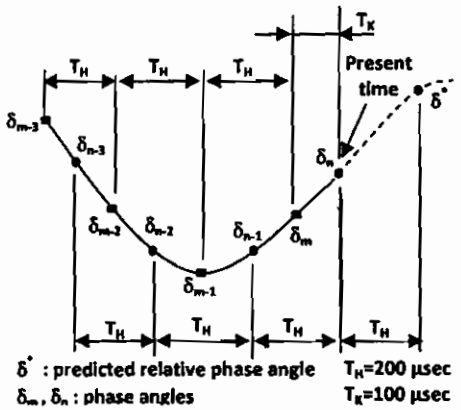

Fig.2 Method of Predicting Phase Difference

The predicted phase difference δ^* for time T_H in the future is derived from the eight pieces of data indicated in Fig.2. These are the phase differences at time T_K before the present time and in addition three values for this time minus increments of time T_H (δ_m, δ_{m-1}, δ_{m-2}, δ_{m-3}) and the phase differences at the current time n and in addition three values for this time minus increments of T_H (δ_n, δ_{n-1}, δ_{n-2}, δ_{n-3}). Equations (7) through (11) are used to perform the calculation.

$$\delta^* = \delta_n + \lambda\, d_n + \mu\, d_{n-1} \quad (7)$$

where,

$$d_n=\delta_n - \delta_{n-1}\ ,\ d_{n-1}=\delta_{n-1} - \delta_{n-2}\ ,\ d_{n-2} = \delta_{n-2} - \delta_{n-3} \quad (8)$$

$$d_m=\delta_m-\delta_{m-1}\ ,\ d_{m-1}=\delta_{m-1}-\delta_{m-2}\ ,\ d_{m-2} = \delta_{m-2} - \delta_{m-3} \quad (9)$$

$$\lambda = (d_n d_{m-2} - d_m d_{n-2})/(d_{n-1} d_{m-2} - d_{m-1} d_{n-2}) \quad (10)$$

$$\mu = (d_{n-1} d_m - d_{m-1} d_n)/(d_{n-1} d_{m-2} - d_{m-1} d_{n-2}) \quad (11)$$

Values of 200 μs and 100 μs were selected for T_H and T_K, respectively, in order to predict accurately.

6.2 Threshold Value (δcritical)

When the predicted phase difference value δ^* obtained by eq.(7) exceeds the setting value ($\delta_{critical}$), it is judged that the generator is unstable. $\delta_{critical}$ is the threshold value used to judge stability. The value for $\delta_{critical}$ is determined by testing the system under varying conditions. The selected value must guarantee operation when the system is unstable and must prevent operation when the system is stable [16].

7. Out-Of-Step Prediction Test Results

The previously explained prediction algorithm was applied to the phase difference between different generator buses of the test systems and the slack bus as recorded by simulating the systems on the PSCAD software. The sampling time was 100 μsec. The following are some results of the proposed algorithm.

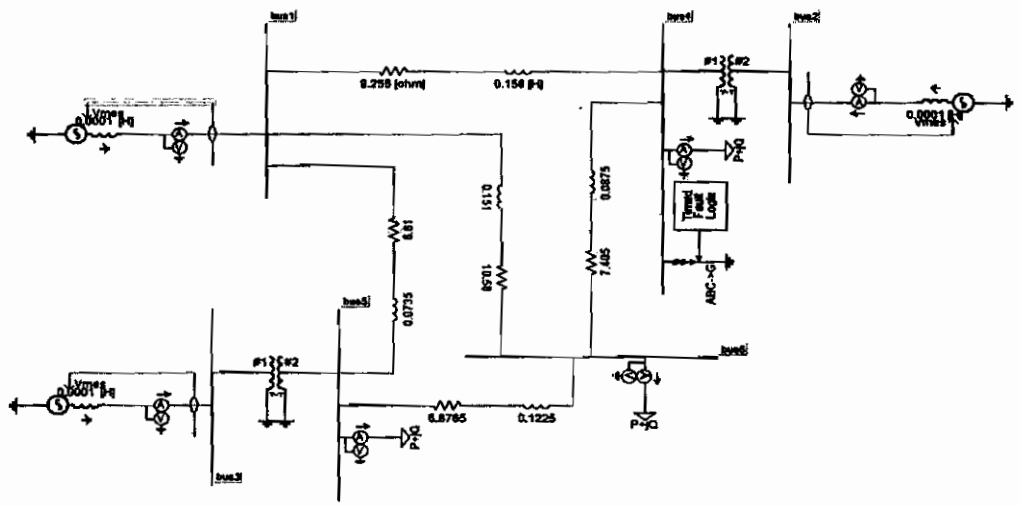

Fig.3 The PSCAD model of the IEEE 6-bus system

7.1 IEEE 6-Bus System

The PSCAD model of the IEEE 6-bus system is shown in Fig.3.

For a three-line-to-ground (3LG) fault at bus 4 the recorded phase difference between Gen.2 and Gen.1 (slack bus generator) is shown in Fig.4.

For a three-line-to-ground (3LG) fault at bus 4 the recorded phase difference between Gen.2 and Gen.1 (slack bus generator) is shown in Fig.4. The predicted phase difference and both recorded and predicted phase difference together are shown in Fig.5 and Fig.6, respectively.

As shown in Fig.6, the predicted and recorded phase difference angles are almost the same, which prove the accuracy of the prediction algorithm used.

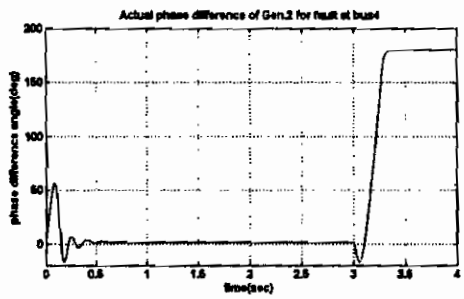

Fig.4 The recorded phase difference between Gen.2 and Gen.1 for a 3LG fault at bus 4

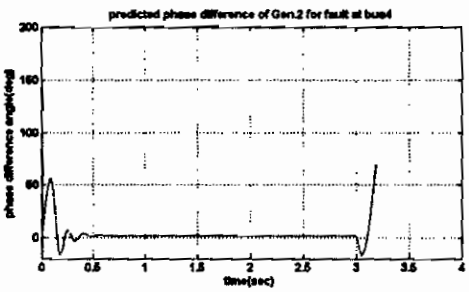

Fig.5 The predicted phase difference between Gen.2 and Gen.1 for a 3LG fault at bus 4

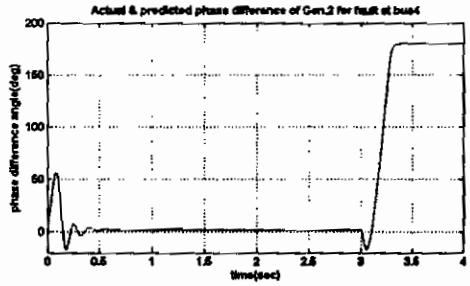

Fig.6 The recorded and predicted phase difference between Gen.2 and Gen.1 for a 3LG fault at bus 4

For the same fault at bus 4 the recorded phase difference between Gen.3 and Gen.1 (slack bus generator) is shown in Fig.7. The predicted phase difference and both recorded and predicted phase difference together are shown in Fig.8 and Fig.9, respectively.

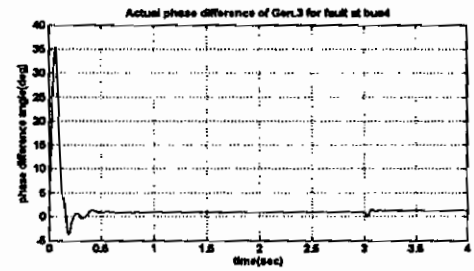

Fig.7 The recorded phase difference between Gen.3 and Gen.1 for a 3LG fault at bus 4

As shown in Fig.9, the predicted and recorded phase difference angles are almost the same, which further prove the accuracy of the prediction algorithm used.
Through several tests of the system during faults of different types and different locations, the minimum threshold value ($\delta_{critical}$) of both generators was found to be 75 deg.

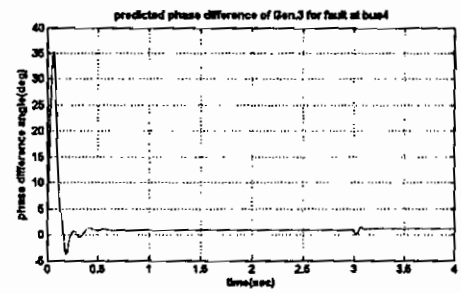

Fig.8 The predicted phase difference between Gen.3 and Gen.1 for a 3LG fault at bus 4

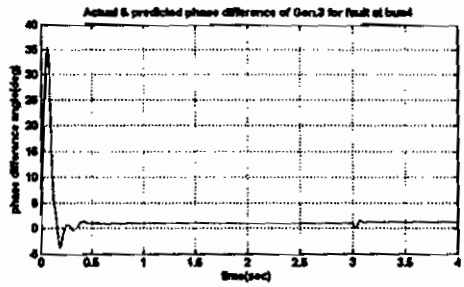

Fig.9 The recorded and predicted phase difference between Gen.3 and Gen.1 for a 3LG fault at bus 4

Referring to Fig.4 and Fig.7, under the same fault condition, Gen.2 will be out of step and Gen.3 will remain stable, where the phase difference angle of Gen.2 exceeded its critical value while that of Gen.3 did not exceed that value.

7.2 IEEE 14-Bus System

The PSCAD model of the IEEE 14-bus system is shown in Fig.10. For a three-line-to-ground (3LG) fault at bus 2 the recorded phase difference between Gen.2 and Gen.1 (slack bus generator) is shown in Fig.11. As shown in Fig.11, Gen.2 will be out of step where its phase difference angle exceeded its critical value.

The predicted phase difference and both recorded and predicted phase difference together are shown in Fig.12 and Fig.13, respectively. As shown in Fig.13, the predicted and recorded phase difference angles are almost the same.

Through several tests of the system during faults of different types and different locations, the minimum threshold value ($\delta_{critical}$) of generator 2 was found to be 60 deg.

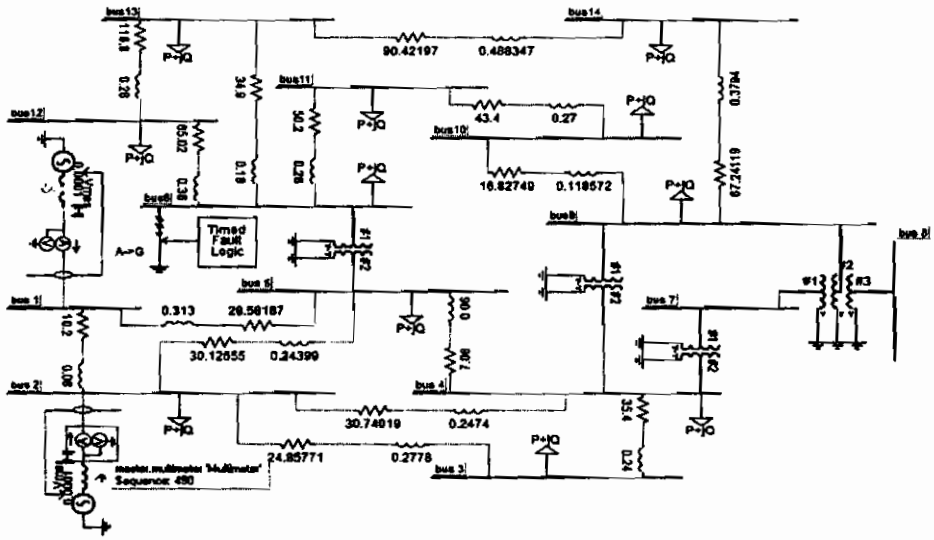

Fig.10 The PSCAD model of the IEEE 14-bus system

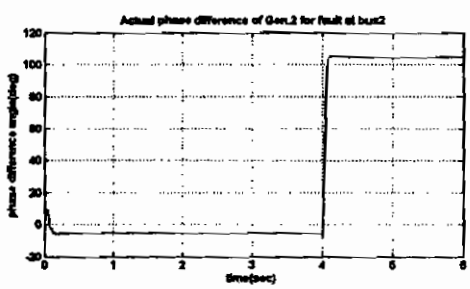

Fig.11 The recorded phase difference between Gen.2 and Gen.1 for a 3LG fault at bus 2

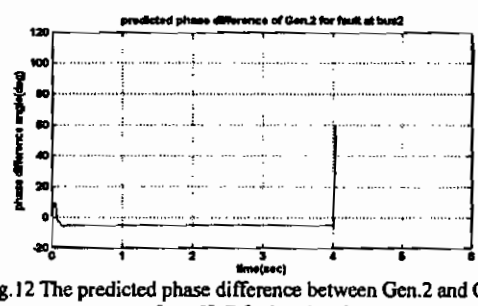

Fig.12 The predicted phase difference between Gen.2 and Gen.1 for a 3LG fault at bus 2

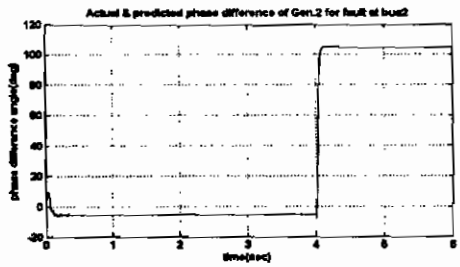

Fig.13 The recorded and predicted phase difference between Gen.2 and Gen.1 for a 3LG fault at bus 2

7.3 Egyptian 500 kV Network

The PSCAD model of the Egyptian 500 kV network is shown in Fig.14. As a sample of test results, the phase difference angles at Gen.3 during 3LG fault at bus 7 will be presented.

For a three-line-to-ground (3LG) fault at bus 7 the recorded phase difference between Gen.3 and Gen.1 (slack bus generator) is shown in Fig.15.

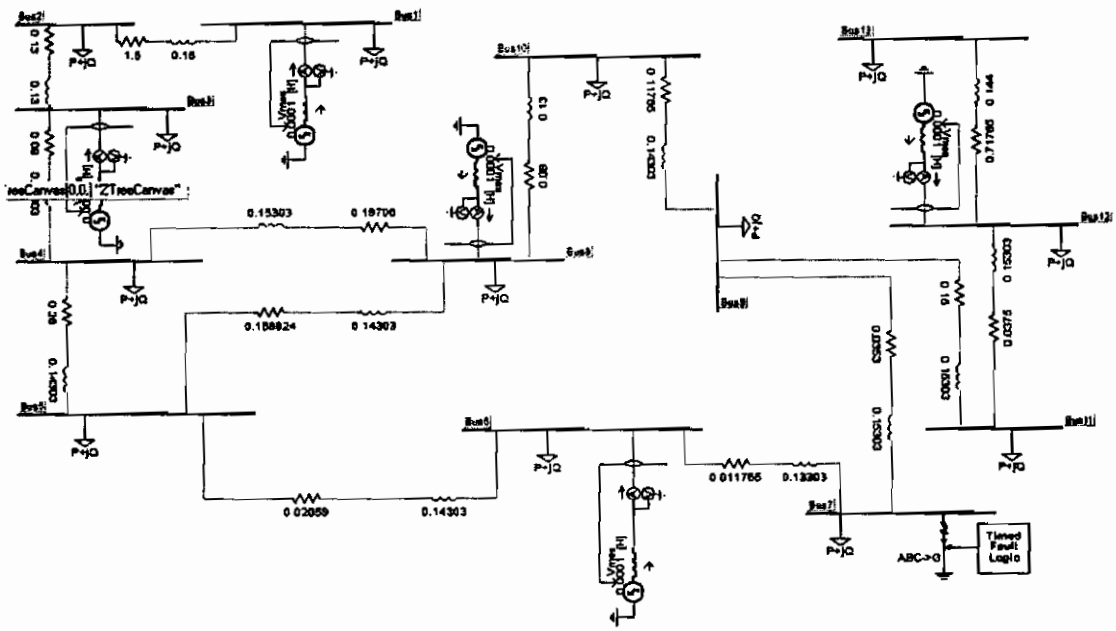

Fig.14 The PSCAD model of the Egyptian 500 kV network

The predicted phase difference and both recorded and predicted phase difference together are shown in Fig.16 and Fig.17, respectively.

Through several tests of the system during faults of different types and different locations, the minimum threshold value ($\delta_{critical}$) of all generators was found to be 50 deg.

As shown in Fig.15, for a 3LG fault at bus 7, Gen.3 will be out of step where its phase difference angle exceeded the critical value.

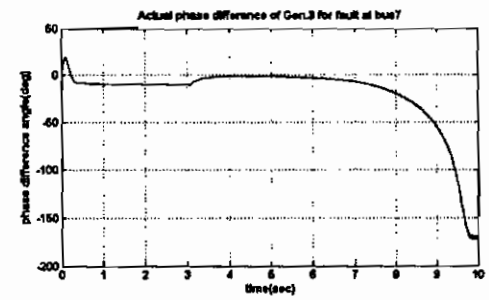

Fig.15 The recorded phase difference between Gen.3 and Gen.1 for a 3LG fault at bus 7

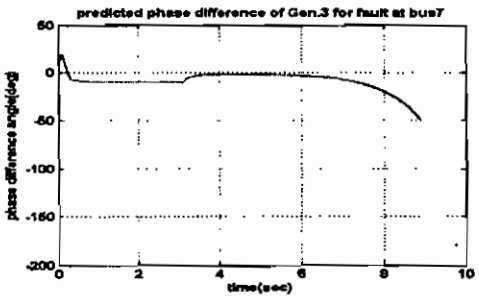

Fig.16 The predicted phase difference between Gen.3 and Gen.1 for a 3LG fault at bus 7

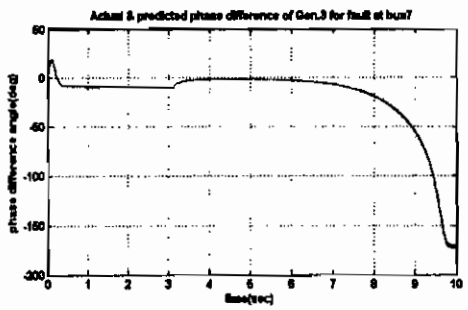

Fig.17 The recorded and predicted phase difference between Gen.3 and Gen.1 for a 3LG fault at bus 7

8. Conclusion

This paper proposed an optimization method for optimal placement of PMUs for complete observability of power system. The proposed method is based on numerical observation and artificial intelligence. The artificial intelligence algorithm used is the ITS algorithm, which is used to find the optimal placement for the PMU to keep the system complete observable. In addition, the paper described a predictive OOS algorithm based on the observation of the voltage phase difference between substations. The proposed optimal placement of PMUs and the OOS algorithms were tested using the IEEE 6 bus, IEEE 14 bus systems and the Egyptian 500 kV network. The test systems were simulated using the PSCAD software program. The placement algorithm and the OOS prediction algorithm were carried out using MATLAB script programs. It was shown by test results the effectiveness of both the PMUs placement and the prediction algorithms introduced.

References

[1] A. G. Phadke, "Synchronized phasor measurements in power systems," *IEEE Comput. Appl. Power*, vol. 6, no. 2, pp. 10–15, Apr. 1993.

[2] T. L. Baldwin, L. Mili, M. B. Boisen, and R. Adapa, "Power system observability with minimal phasor measurement placement," *IEEE Trans. Power Syst.*, vol. 8, no. 2, pp. 707–715, May 1993.

[3] R. F. Nuqui and A. G. Phadke, "Phasor measurement unit placement techniques for complete and incomplete observability," *IEEE Trans. Power Del.*, vol. 20, no. 4, pp. 2381–2388, Oct. 2005.

[4] B. Milosevic and M. Begovic, "Nondominated sorting genetic algorithm for optimal phasor measurement placement," *IEEE Trans. Power Syst.*, vol. 18, no. 1, pp. 69–75, Feb. 2003.

[5] B. Xu and A. Abur, "Optimal placement of phasor measurement units for state estimation," *Final Project Report, PSERC*, Oct. 2005.

[6] B. Xu and A. Abur, "Observability analysis and measurement placement for systems with PMUs," in *proc. IEEE Power Eng. Soc. Power Systems Conf. Expo.*, Oct. 2004, pp. 943–946.

[7] C. Rakpenthai, S. Premrudeepreechacharn, S. Uatrongjit, and N. R. Watson, "An optimal PMU placement method against measurement loss and branch outage," *IEEE Trans. Power Del.*, vol. 22, no. 1, pp. 101–107, Jan. 2005.

[8] S. H. Horowitz, A. G. Phadke, *Power System Relaying*, John Wiley&Sons, New York, 1995.

[9] C.W. Taylor, J.M. Haner, L.A. Hill, W.A. Mittelstadt and R.L. Cresap, "A new OS relay with rate of change of apparent resistance augmentation", *IEEE Trans. On Power Systems*, Vol. PAS-102, No. 3, Mar. 1983, pp. 631-639.

[10] W.R. Roemish, E.T. Wall, "A new synchronous generator out-of-step relay scheme. Part I Abbreviated version", *IEEE Trans. On Power Systems*, Vol. PAS- 104, No. 3, March 1985, pp. 563-571.

[11] T.L. Baldwin, L. Mili, R. Adapa " Power system observability with minimal phasor measurement placement " *IEEE Trans. On power system*, vol. 8, no. 2, May 1993.

[12] B.Gou and A.Abur, "A direct numerical method for observability analysis", *IEEE Trans. on Power Systems*, vol.15, no.2, May 2000.

[13] F. Glover "Tabu Search: Part I," ORSA J. Comput., vol.1, no.3, pp. 190-206, 1989.

[14] F.Glover " Tabu Search: Part II," ORSA J. Comput., vol.2, no.1, pp. 4-32, 1990.

[15] W.Lin, F.Cheng and M.Tsay, "An improved tabu search for economic dispatch with multiple minima", *IEEE Trans. On Power Systems*, vol. 17, no. 1, pp. 108–112, Feb. 2002.

[16] Y. Ohura, M. Suzuki, K. Omata " A predictive out-of-step protection system based on observation of the phase difference between substations " *IEEE Trans. On Power Delivery*, vol. 5, no. 4, Nov. 1990.